



## Experimental study: Underwater propagation of polarized flat top partially coherent laser beams with a varying degree of spatial coherence

S. Avramov-Zamurovic<sup>a,\*</sup>, C. Nelson<sup>b</sup>

<sup>a</sup> Weapons and Systems Engineering Department, US Naval Academy, 105 Maryland Avenue, Annapolis, MD 21402, USA

<sup>b</sup> Electrical and Computer Engineering Department, US Naval Academy, 105 Maryland Avenue, Annapolis, MD 21402, USA

### ARTICLE INFO

#### Keywords:

Polarization  
Underwater laser propagation  
Partial spatial coherence  
Multi-Gaussian Schell model beam  
Scintillation

### ABSTRACT

We report on experiments where spatially partially coherent laser beams with flat top intensity profiles were propagated underwater. Two scenarios were explored: still water and mechanically moved entrained salt scatterers. Gaussian, fully spatially coherent beams, and Multi-Gaussian Schell model beams with varying degrees of spatial coherence were used in the experiments. The main objective of our study was the exploration of the scintillation performance of scalar beams, with both vertical and horizontal polarizations, and the comparison with electromagnetic beams that have a randomly varying polarization. The results from our investigation show up to a 50% scintillation index reduction for the case with electromagnetic beams. In addition, we observed that the fully coherent beam performance deteriorates significantly relative to the spatially partially coherent beams when the conditions become more complex, changing from still water conditions to the propagation through mechanically moved entrained salt scatterers.

### 1. Introduction

Propagation of laser light through random media [1,2] is of great interest in developing a more complete understanding of the properties of laser light intensity fluctuations in all practical laser applications. Much of the recent research focus has been on laser propagation through turbulent atmospheric conditions, with an emphasis on laser light scintillation mitigation by source partial coherence [3–5], aperture averaging [6], sparse aperture detectors [7,8], wavelength diversity [9], source temporal variations [10], and polarization diversity [11–13]. The study of laser light propagation underwater is of significant importance for communication and sensing applications, in particular with submersible robots [14–17], but there are significant challenges in light intensity distortion mitigation that require detailed studies. Some of the challenging aspects of the underwater environment for laser propagation include interactions with the sea surface, multipath propagation, intensity fluctuations due to the index of refraction changes caused by temperature variation along the propagation path, and the scattering of light off particulates in the water. Background research on light scintillation in the ocean has been theoretically studied for plane, spherical, and Gaussian beams [18], and for partially coherent beams [19]. To the best of our knowledge, mitigation techniques using polarization diversity have not been experimentally explored in detail for the underwater

environment. Our motivation to experiment with propagation of laser light underwater stems from our interest in applying to an underwater medium, source partial coherence variations and polarization diversity techniques that have been successfully implemented in reducing the scintillation of the laser light in a turbulent atmosphere [20–22]. These techniques are based on a statistical treatment of a complex propagating medium, and as such show the potential to improve the properties of laser light propagating in a complex underwater environment.

Multi-Gaussian Schell Model (MGSM) spatially partially coherent beams (PCB) [23] with a varying degree of spatial coherence have a flat top intensity profile, and can be created by a straightforward technique utilizing a spatial light modulator (SLM) which allows an effective spatial degree of coherence manipulation. Experimentally, the coherent laser beam is redistributed into independent beamlets by interacting with phase screens on the spatially distributed liquid crystal cells of the SLM. True PCBs theoretically require statistical realizations on an SLM changing at an infinite rate [24], which is not currently realizable with available instrumentation. Therefore, for our experiments we generate pseudo partially coherent beams (PPCBs) which describe a beam made using a finite cycling rate of SLM phase screens. Statistically, the propagation of spatially distributed beamlets with a random phase through complex medium results in a more even laser light intensity

\* Corresponding author.

E-mail address: [avramov@usna.edu](mailto:avramov@usna.edu) (S. Avramov-Zamurovic).

distribution on the target. This method constructs uniformly polarized scalar laser beams with varied source partial coherence.

Electromagnetic spatially partially coherent laser beams are constructed from the combination of horizontally and vertically polarized scalar beams [12,25,26]. It has been theoretically and experimentally [20,21,27] shown, in optical atmospheric turbulence, that electromagnetic spatially PCBs have a reduced scintillation index of up to 50% as compared to the scalar beams, but to our knowledge, this property has not been explored in an underwater environment. The basis for such a high reduction in laser light intensity fluctuations is related to the property that adding vertically and horizontally PCBs results in an arbitrary polarization of electromagnetic beam. The scalar beams in this experiment have a well-defined single angle polarization (vertical or horizontal) and their scintillation is related to both the induced variations from the cycling of the screens that produce the partial spatial coherence and the interaction of the laser beam with the water and moving entrained scatterers along the path of propagation. The constructed electromagnetic beams have the same spatial coherence as the scalar beams, propagate through the same environment, but also have a random phase. This randomization of the polarization effectively increases the chances of spatially distributed beamlets, to on average have reduced constructive and destructive interference at the target after propagation through a random medium.

Our experiments explore laser light intensity fluctuations, when electromagnetic spatially partially coherent MGSM beams with varying degrees of source coherence are propagated underwater in two different media scenarios: still water and water with moving entrained salt scatterers. Since, to the best of our knowledge, there are no theoretical derivations for our experimental setup, our measurement expectations are motivated on the results achieved from propagation through atmospheric turbulence [11,12]. Further, we do not claim a direct comparison between the atmospheric and underwater laser light scintillation, but simply present our observations and intuition of the measurements in the underwater conditions. Our findings support similar trends in measured scintillation for both environments, and thus suggest that the polarization diversity technique is a potentially viable performance mitigation technique in the underwater environment. We clearly observed a 50% scintillation reduction for electromagnetic beams as compared with scalar beams underwater, and this result matches the atmospheric research.

The paper is organized as follows. Beam generation is presented in Section 2. The experimental setup is discussed in Section 3. In Section 4 we describe the data analysis. In Section 5 we discuss results, and in Section 6 conclusions.

## 2. Beam generation

### 2.1. Scalar MGSM beams

In this paper we will provide a brief overview of the theory behind the generation of the MGSM [23,28–31].

The second-order correlation properties of a wide-sense statistically stationary electromagnetic beam can be described by means of the beam coherence-polarization matrix or cross-spectral density matrix [11,12] whose spatial counterparts have the same form.

A recently developed model for the MGSM (flat top) beams, gives the following spectral (scalar) degree of coherence:

$$\mu^{(0)}(\rho_1, \rho_2) = \frac{1}{C_0} \sum_{m=1}^M \binom{M}{m} \frac{(-1)^{m-1}}{m} \exp\left[-\frac{|\rho_2 - \rho_1|^2}{2m\delta^2}\right], \quad (1)$$

where  $\rho_1$  and  $\rho_2$  are position distances and superscript (0) refers to the source plane,

$$C_0 = \sum_{m=1}^M \binom{M}{m} \frac{(-1)^{m-1}}{m}, \quad (2)$$

is the normalization factor used for obtaining the same maximum intensity level for any number of terms  $M$  in the summation, where  $\binom{M}{m}$  is the binomial coefficient. In Eq. (1),  $\delta$  is the r.m.s. width of the degree of coherence which describes the degree of coherence of the beam; where a value of  $\delta = 0$  gives a spatially incoherent beam and a value of  $\delta \rightarrow \infty$  gives a spatially coherent beam. Additionally, the upper index  $M$  relates to the flatness of the intensity profile formed in the far field:  $M = 1$  corresponds to the classical Gaussian Schell-Model source and  $M \rightarrow \infty$  corresponds to sources producing far fields with flat centres and abrupt decays at the edges.

It is important to note that we constructed the electromagnetic beams using the orthogonal components, namely vertically and horizontally polarized scalar beams are optically combined by means of interferometry. In this case the same scalar degree of coherence is used for both the vertically and horizontally polarized beams as described in Eqs. (1) and (2). Ref. [25] provides extensive details on the cross spectral density of the electromagnetic beams and provides the foundation for the construction of the electromagnetic beams used in this paper. Specifically, Ref. [25], Eqs. 19–21 provide the cross spectral density matrix of the electromagnetic Multi-Gaussian Schell Model beam.

Ref. [23] provides general details on how one uses Eqs. (1) and (2) to generate MGSM spatially partially coherent beams by using an SLM. Additionally, the SLM phase screens were created in order to shift the first order ‘hot spot’ off of the beam propagation path utilizing a method developed by Hyde et al. in [32–34] and further described for use with SLMs in [35].

### 2.2. Scintillation index of the electromagnetic beams with uncorrelated orthogonal field components

The following discussion gives a theoretical summary on calculating the scintillation index of an electromagnetic beam, [11,12,25–27,36,37]. The conventional measure of the intensity fluctuations at a single position in an optical wave is its normalized variance or the scintillation index (SI), defined as

$$SI = c(\mathbf{r}) = \frac{i^{(II)}(\mathbf{r}) - [i^{(I)}(\mathbf{r})]^2}{[i^{(I)}(\mathbf{r})]^2}, \quad (3)$$

where  $i^{(II)}(\mathbf{r}) = \langle i(\mathbf{r})^2 \rangle$  and  $i^{(I)}(\mathbf{r}) = \langle i(\mathbf{r}) \rangle$  are the second and the first moment of the instantaneous intensity,  $i(\mathbf{r})$ , and  $\mathbf{r}$  is the position vector. As was shown in [11], the scintillation index of an electromagnetic beam may be expressed in the more general form:

$$c(\mathbf{r}) = \frac{c_{xx}(\mathbf{r})[i_x^{(I)}(\mathbf{r})]^2 + 2c_{xy}(\mathbf{r})i_x^{(I)}(\mathbf{r})i_y^{(I)}(\mathbf{r}) + c_{yy}(\mathbf{r})[i_y^{(I)}(\mathbf{r})]^2}{[i_x^{(I)}(\mathbf{r}) + i_y^{(I)}(\mathbf{r})]^2} \quad (4)$$

In this representation  $i_x^{(I)}$  and  $i_y^{(I)}$  are the mean value of intensities of  $x$  and  $y$  components of the electric field while,  $c_{xx}(\mathbf{r})$ ,  $c_{yy}(\mathbf{r})$  are the scintillation indices of the field components fluctuating in two orthogonal directions and  $c_{xy}(\mathbf{r})$  is that for their mutual scintillation index:

$$c_{xy}(\mathbf{r}) = \frac{\langle i_x(\mathbf{r})i_y(\mathbf{r}) \rangle - i_x^{(I)}(\mathbf{r})i_y^{(I)}(\mathbf{r})}{i_x^{(I)}(\mathbf{r})i_y^{(I)}(\mathbf{r})} \quad (5)$$

For uncorrelated field components,  $c_{xy}(\mathbf{r})$  vanishes and leads to a reduction in the scintillation index compared to that for fully or partially correlated field components. In the limiting case of an unpolarized light beam, i.e., that with uncorrelated electric field components with equal intensities  $i_x = i_y$ , the scintillation index can be readily shown to be reduced by a factor of two, compared to an equivalent polarized (scalar) beam [11,12].

The reduction of the scintillation index was found using the following formula

$$R = \frac{\frac{c_{xx}(\mathbf{r})+c_{yy}(\mathbf{r})}{2} - c(\mathbf{r})}{\frac{c_{xx}(\mathbf{r})+c_{xx}(\mathbf{r})}{2}}. \quad (6)$$

**Table 1**  
Polarimeter measurements.

Scalar beam: Vertical polarization	Scalar beam: Horizontal polarization	Electromagnetic beam
S1 -0.9995	S1 0.998	S1 -0.041
S2 -0.007	S2 -0.026	S2 -0.23
S3 -0.032	S3 -0.06	S3 -0.9723
DOP 97.6%	DOP 102.4%	DOP 83.7%
Power -37.3 dB	Power -38 dB	Power -34.8 dB

### 3. Experimental set-up

A stabilized 2 mW He–Ne laser light source (see Fig. 1.), *A*, at 632.8 nm was expanded, *B*, to fill an SLM, *C*, window with spatial resolution of  $256 \times 256$  pixels, and a sensor area of 6.14 mm x 6.14 mm. Eight thousand screens in one experimental case and two thousand screens in the other case, with prescribed statistics to define spatial degree of coherence (see Eqs. (1), (2)) and cycling at the rate of 333 Hz, were used to generate the PPCBs.

As shown in Fig. 1, a linear polarizer,  $D_1$ , was used to verify a vertical polarization after the SLM. Next, the beam was split at the first 50:50 beam splitter,  $E_1$ , with the reflected path subsequently reflecting from a mirror,  $H_2$ , going through a second linear polarizer,  $D_2$ , to ‘lock-in’ the vertical polarization. This vertically polarized beam was then combined with the transmission path at the second 50:50 beam splitter,  $E_2$ . For the transmitted path from the first beam splitter, the laser light went through a half-wave plate,  $F$ , to rotate the polarization to horizontal, and then through an ND filter,  $G$ , to help synchronize the intensities between the two paths. Next, the reflected horizontally polarized beam from mirror,  $H_1$ , was combined with the vertically polarized light at the second beam splitter,  $E_2$ , and thus creating the electromagnetic beam. The polarizations were confirmed with a polarimeter,  $I$ , and the baseline results are shown in Table 1. The neutral density filter was inserted in the ‘horizontal’ or transmission branch in order to match light intensity from each path and form the most effective electromagnetic beam.

In order to eliminate the zeroth order ‘hot spot’ generated by the SLM, a mechanical iris,  $L$ , was used to isolate the first order beam from the rest. Additionally, to allow for full development of the PPCB the beam was propagated approximately 5 m with the use of a mirror,  $H_3$ , prior to entering the water tank.

The Stoke’s parameters:  $S_1$ ,  $S_2$  and  $S_3$  achieved in our experiments are given in Table 1 and show a good agreement with theoretical polarization requirements of the electromagnetic PPCB [38]. The power match between the vertically and horizontally polarized beams is within 2% as measured in dB, or 16% as measured in mW. The electromagnetic beam power matches the sum of the scalar beams within 5% as measured in mW. The intensity match among the laser beams demonstrates a good alignment of the electromagnetic beam composition.

The tank,  $J$ , used was 76 cm long, 30 cm wide and filled with 38 litres of distilled water with an added 300 g of sea salt. The tank was kept at a constant room temperature (20 °C), [39,40], and while the scattering was primarily from entrained salt there were a few additionally scatterers noted from dust particles and similar airborne dirt. A mechanical agitator moved the water with entrained salt scatterers in it. The propagation laser light intensity data was collected after approximately 20 min to ensure steady state motion in the tank. We specifically constructed a propagation medium to study the effects of entrained salt on laser propagation. Practically, we used the few dust particulates to estimate water motion.

The mechanical agitator was used in a slow and fast mode during the experiments. In the slow mode the general estimated speed of motion was on the order of 3–5 mm/s and in the fast mode approximately 50–70 mm/s. These estimates for speed of motion were derived by measuring displacement of an Airy ring, produced by a moving scatterer as imaged in two consecutive frames using the camera in the direct path of the propagation. Additionally, a number of such measurements were

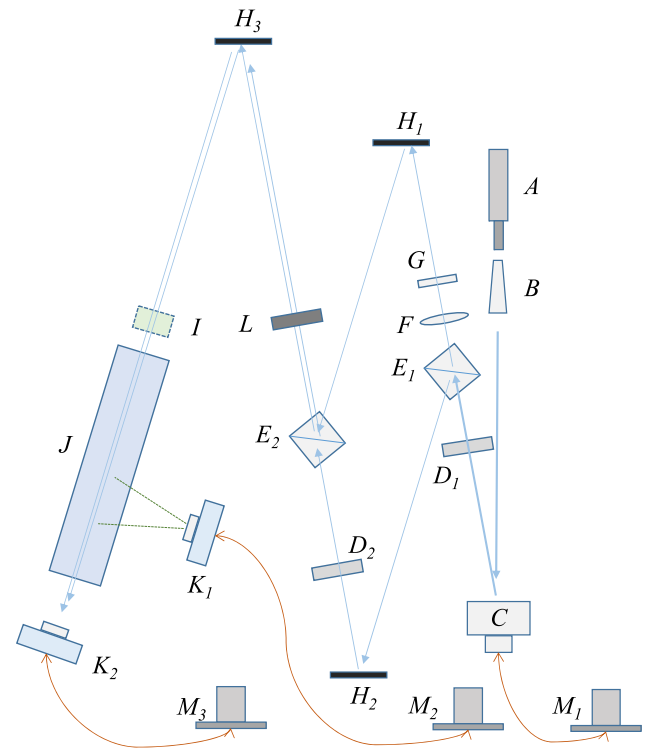


**Fig. 1.** Experimental setup - *A* — HeNe laser, *B* — beam expander, *C* — spatial light modulator,  $D_{1,2}$  — linear polarizer,  $E_{1,2}$  — beam splitter,  $F$  — half-wave plate,  $G$  — neutral density filter,  $H_{1,2,3}$  — mirror,  $I$  — polarimeter (inserted before testing),  $J$  — 1 m propagation tank,  $K_{1,2}$  — camera,  $L$  — mechanical iris, and  $M_{1,2,3}$  — computer.

averaged in order to obtain a reliable estimate of the general motion in the tank in slow and fast mode scenarios.

It should be noted that the underwater propagation medium was kept the same for all performed experiments. Our findings compare the relative scintillation performance among the laser beams with different polarizations and different degrees of coherence propagating under the same environmental conditions.

The laser light intensity fluctuations were recorded using two cameras,  $K_{1,2}$ , where the first camera was positioned directly on the axis of the light propagation with neutral density filters used to prevent saturation. The second camera was positioned perpendicularly to the propagation of the beam path and used to estimate the relative movement of the scatterers under the different environmental conditions. The camera sensor spatial resolution of  $480 \times 640$  pixels, each size  $7.4 \mu\text{m}$ , provides the beam observation area of  $3.552 \text{ mm} \times 4.736 \text{ mm}$ , and the sensor has an intensity resolution of 14 bits. The range of spatial coherence width radii tested in this experiment covered 8 different values from 0.1 mm to 1.1 mm, which was acceptable for the given sensor size. Additionally, for each data run, approximately 1000 images were collected at a rate of 10 Hz, with an exposure time of 100 ms. This recording rate ensures that  $\sim 30$  frames cycled by SLM were averaged, providing reasonable theoretical conditions for the analysis of PPCBs [40,41].

### 4. Data analysis

The focus of our data analysis is the measurement of average light intensity and its variations across the sensor area.

The first step is the representation of the mean scattered intensity,  $I_{avg}$ , from the beam propagating through the water. It is important to note that the background noise has been eliminated from all of the analysed images. The images in Fig. 2 show a matrix representation of

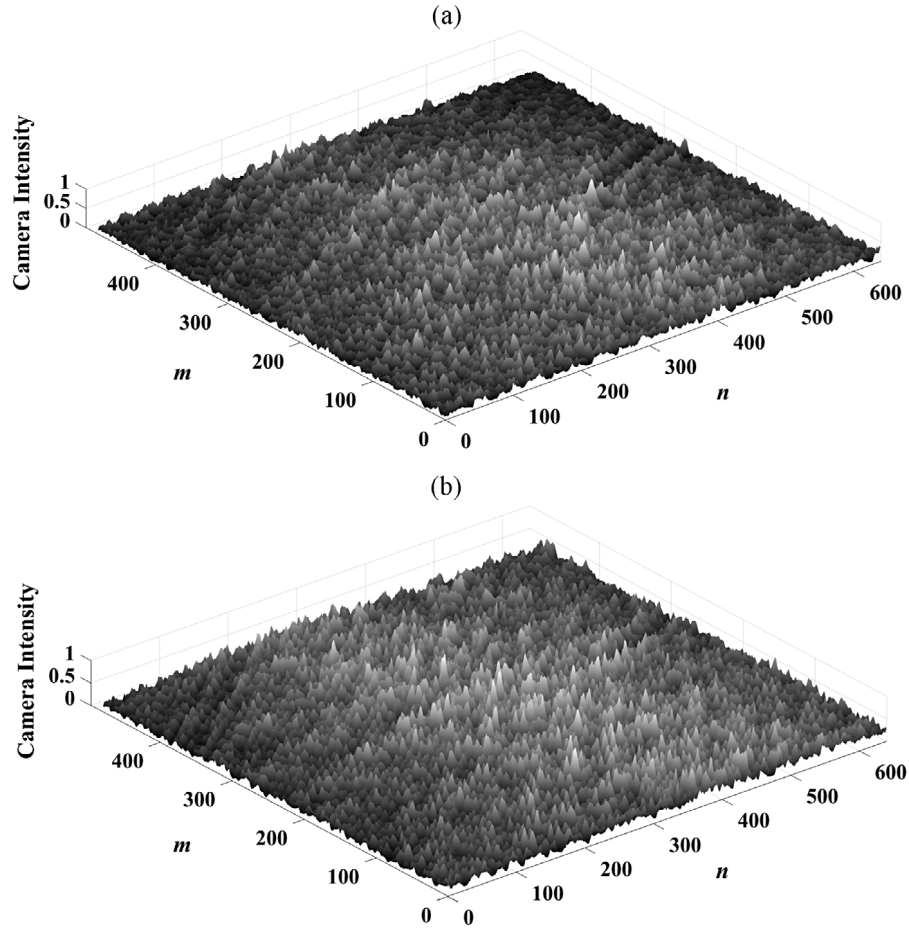


**Fig. 2.** Mean light intensity  $I_{avg}$  across the sensor area: (a) still conditions  $MI_{avg} = 1$  (units) with the standard deviation across the sensor area of 0.083 (units), (b) mechanically agitated (fast mode) conditions  $MI_{avg} = 0.76$  (units) with the standard deviation across the sensor area of 0.075 (units). The images are normalized to the still condition values in order to show the spatial beam spread.

the light,  $I_{avg}$  from the electromagnetic MGSM beam with a coherence width,  $\delta$ , of 0.77 mm in still and mechanically agitated conditions (fast mode). It is apparent that the beam is visible at the middle of the image, with some practical filtering artefacts. The objective of Fig. 2 is to showcase that the overall beam spreading between experimental cases is not significant over the propagation path length of the experiment. The overall normalized intensity was reduced once the underwater conditions became mechanically agitated. Assuming that each image,  $(im)$ , is an  $m \times n$  matrix, with  $m = 480$  and  $n = 640$ , and that there are  $N = 1000$ , images taken we find the matrix  $I_{avg}$  as:

$$I_{avg} = \frac{\sum_{j=1}^N (im)_j}{N} \quad (7)$$

The image of  $I_{avg}$  serves as an insight into the beam quality at the target.

Additionally, to obtain an overall single value comparative parameter,  $MI_{avg}$ , the mean value of  $I_{avg}$  is calculated.  $MI_{avg}$  represents the total ‘raw’ averaged intensity:

$$MI_{avg} = \frac{\sum_{k=1}^n \sum_{j=1}^m I_{avg,j,k}}{nm} \quad (8)$$

The parameter  $MI_{avg}$  will be used to numerically compare the propagation of the laser beams in various underwater conditions.

The spatial variance of the laser light intensity fluctuations across the sensor area with the background adjustment,  $B_{avg}$ , applied to each image is calculated as the scintillation index  $SI_B$ :

$$SI_B = \frac{\sum_{i=1}^N ((im_i - B_{avg}) - (I_{avg} - B_{avg}))^2}{N (I_{avg} - B_{avg})^2} \quad (9)$$

where  $B_{avg}$  is a single value parameter representing the average background intensity.

To obtain a single parameter representing  $SI$  (see Eq. (3)) we find the average value  $MSI_{Bavg}$

$$MSI_{Bavg} = \frac{\sum_{k=1}^n \sum_{j=1}^m SI_{Bj,k}}{nm} \quad (10)$$

Fig. 3 represents the scintillation index across the sensor in still and fast moving mechanically agitated conditions. The increase in scintillation between Fig. 3a and Fig. 3b (going from  $MSI_{Bavg} = 0.059$  to  $MSI_{Bavg} = 0.08$ ) is significant since the standard deviation of the measurements across the whole sensor is low.

Fig. 4 shows a typical distribution of the scintillation index calculated for each pixel, as a function of measured camera light intensity (non-normalized). The correlation between the low intensity camera measurements and the calculated scintillation was observed. In order to eliminate this dependence, the scintillation index for the intensities lower than 1000 units were eliminated from the pool used for the calculation of  $MSI_{Bavg}$ . That said, it is important to mention that the measured trends reported do not change even if this precaution is not implemented, due to the very high number of realizations used to derive statistics (307,200). During the testing, the intensity of the light on the camera sensor was kept constant (in the middle of the full camera range) by the use of neutral density filters. Additionally, we also selected only a part of the sensor to test the dependency of the results on the location of the beam on the sensor. Calculated scintillation trends for the cut-out sensor were exactly the same as for the whole sensor area. These various analysis steps were implemented in order to establish the reliability of our observations.

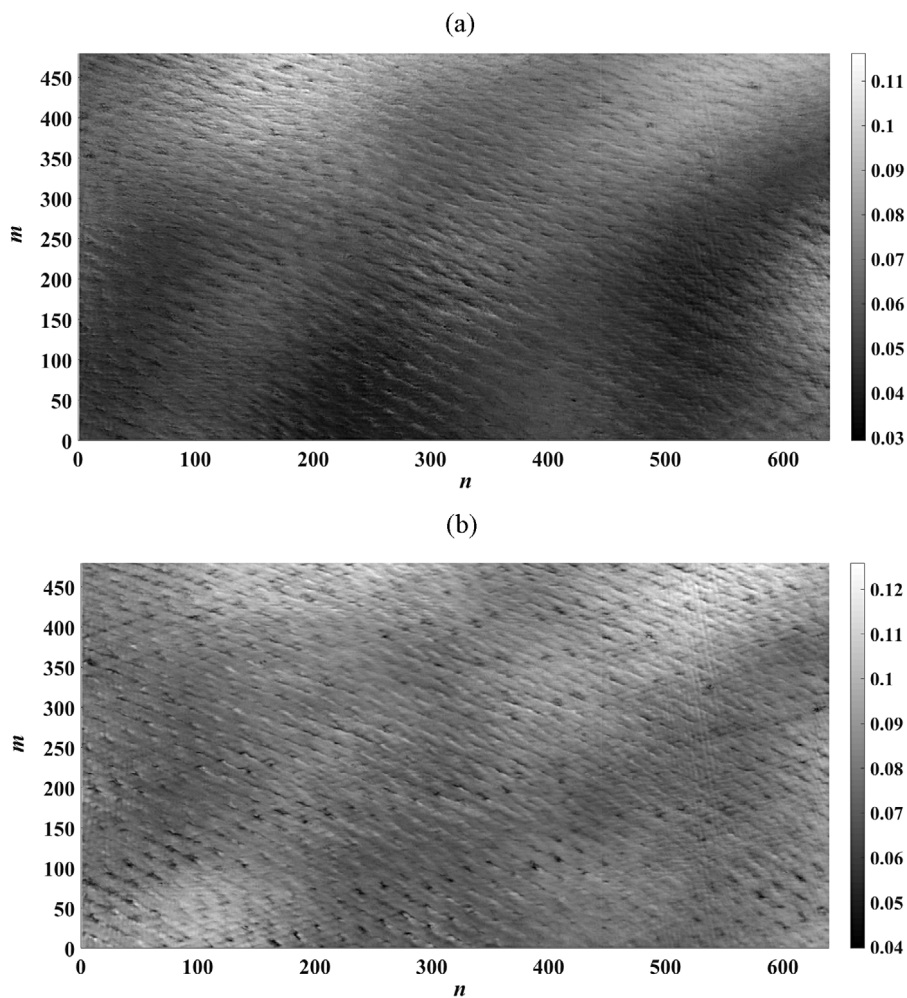


Fig. 3. Scintillation index  $SI_B$  across the sensor area for MGSM coherence width,  $\delta$ , 0.77 mm: (a) still conditions  $MSI_{Bavg} = 0.059$  with the standard deviation across the sensor area of 0.0124, (b) mechanically agitated (fast mode) conditions  $MSI_{Bavg} = 0.08$  with the standard deviation across the sensor area of 0.0074.

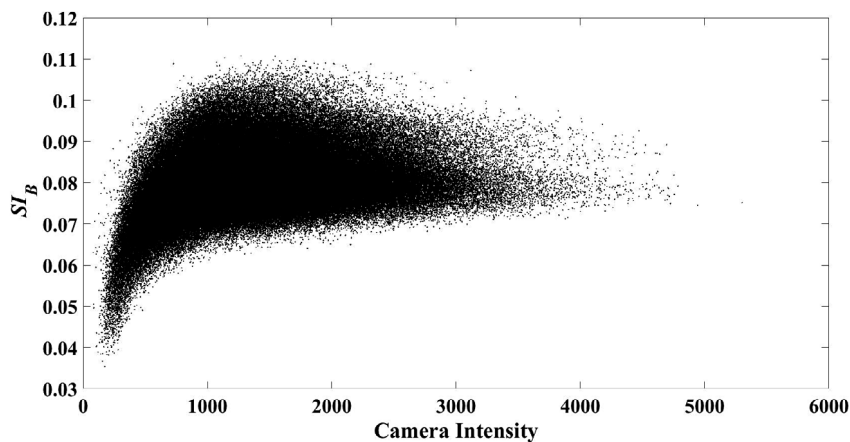


Fig. 4. Dependence of the scintillation index,  $SI_B$ , on the measured light intensity for the electromagnetic MGSM beam with coherence width,  $\delta$ , of 0.77 mm for the mechanically agitated conditions (fast mode). Measured  $MSI_{Bavg} = 0.08$  units with the standard deviation of 0.0074 units. Note, the total number of measurements was 307,200.

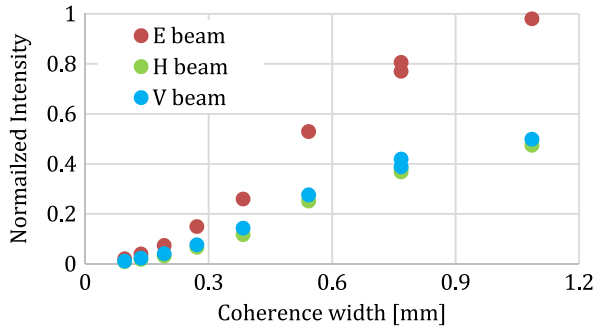


Fig. 5. Average light intensity  $MI_{avg}$  measured across the sensor for still conditions for each light polarization as a function of coherence width,  $\delta$ . Where, E beam is an electromagnetic beam, and V beam and H beam are vertically and horizontally polarized scalar beams respectively.

## 5. Results

We present measured light intensities and their variations, and the scintillation index for spatially partially coherent beams with varied spatial coherence widths and polarization, and also Gaussian beams.

Note that,  $\delta$  was defined in Eq. (1) as the r.m.s. width of the degree of coherence and it is labelled coherence width in the figures.  $\delta$  is calculated from the SLM resolution and number of pixels used in the construction of the SLM screen and is described in [22].

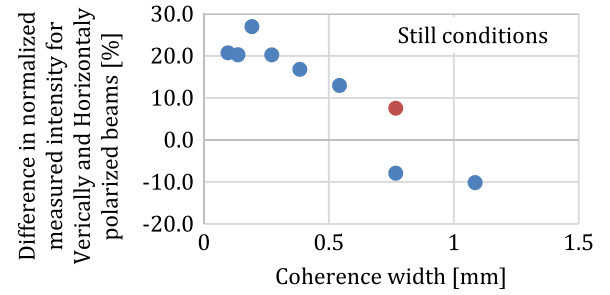
### 5.1. Electromagnetic spatially partially coherent beams with flat top profile

Fig. 5 represents the scope of the experiments in terms of the MGSM beam spatial coherence width sizes tested as well as relative intensity values recorded. The most significant feature is a linear increase in the intensity as the beams become more coherent. The measurements are shown in normalized units to the most spatially coherent E beam. Note that there are two measurements taken for a coherence width,  $\delta$ , size 0.77 mm due to the change in the number of screens cycled for the coherence width radii 0.77 mm case. Seven of the measurements were taken with 8000 phase screens and two sets with 2000 phase screens (0.77 mm and the 1.09 mm cases), where the 0.77 mm case overlapped with the 8000 phase screens to show consistency in the data measurements. Fig. 5 shows that the change in number of cycled screens does not influence the intensity measurements.

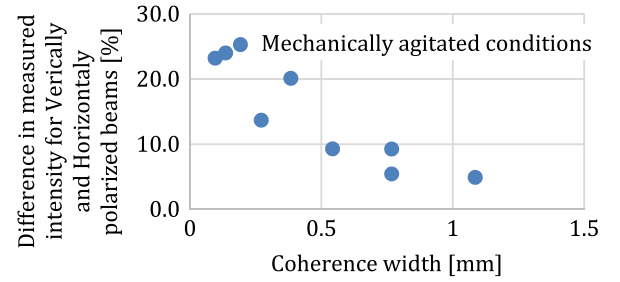
Fig. 6 shows that the measured intensity for vertically and horizontally polarized beams slightly differ as a function of coherence width. The trend is similar between still and agitated conditions, with the larger differences showing for the less spatially coherent beams, and more agreement when more spatially coherent beams are propagated. While this difference should have remained constant over the scope of experimentation, it has to be taken into the consideration that there was a slight mismatch between the vertical and horizontal scalar beams as suggested using the polarimeter. That said the measurements in Fig. 6 suggest a possible dependence of the measured intensity on the spatial coherence of the beam.

Fig. 7 shows measured  $MSI_{Bavg}$  for typical agitated conditions, and Table 2 summarizes the effect of polarization on scintillation in terms of how much the scintillation is decreased when the intensity fluctuations for scalar and electromagnetic beams are compared. Measured reduction, MR, as given in Table 2, and is based on actual measurements of the scintillation of the electromagnetic beam  $MSI_{BavgEbeam}$ , and the scalar beams  $MSI_{BavgVertical}$  and  $MSI_{BavgHorizontal}$ :

$$MR = \frac{\frac{MSI_{BavgVertical} + MSI_{BavgHorizontal}}{2} - MSI_{BavgEbeam}}{\frac{MSI_{BavgVertical} + MSI_{BavgHorizontal}}{2}} \quad (11)$$



(a)



(b)

Fig. 6. Measured intensity difference between the vertically and horizontally polarized light, as a function of coherence width in (a) still, and (b) mechanically agitated conditions. Note, a red labelled data point outlier in Fig. 6a. (For interpretation of the references to colour in this figure legend, the reader is referred to the web version of this article.)

Eq. (4) gives a method to calculate the  $SI$  for the electromagnetic beam in atmospheric turbulence based on the intensity and the scintillation of the scalar beams and thus reduction given in Eq. (6) depends only on the scalar beam performance. Eq. (11) uses the measured  $SI$  for both scalar and electromagnetic beams.

The significance of this result is that we have experimentally measured about a 50% reduction for the beams propagating underwater in still conditions and about a 40% reduction in agitated conditions. This finding demonstrates the possibility to use the polarization diversity for mitigating some of the deterioration effects on laser light propagation in an oceanic environment. Interestingly, in still water the reduction in scintillation is consistent and more closely follows the theory derived for the spatially PPCBs propagating in atmospheric optical turbulence. Measured scintillation in mechanically agitated water does not only depend on imperfection in electromagnetic beam generation due to the finite SLM cycling rate, but also potentially on some multi-path propagation created by moving entrained scatterers. As a consequence, the scintillation index is generally higher in mechanically agitated water, and the observed scintillation reduction is less.

Fig. 8 shows the standard deviation of the  $MSI_{Bavg}$  measurements and it demonstrates the confidence in the presented results. Based on the measurement uncertainty as demonstrated with the standard deviation values, it is possible to confidently estimate the performance trends from our results.

Fig. 9 shows the comparison of  $MSI_{Bavg}$  for the still and mechanically agitated conditions with mechanically agitated fast moving entrained scatterers. Note the match in the performance of both scalar beams in respective conditions. Measurements clearly show a substantial reduction in scintillation on the order of 50% when scalar beams are compared to the electromagnetic beams for the full range of coherence width values and water conditions.

Fig. 10 shows the ratio between the scintillation in agitated conditions and still conditions. The ratio shows how much stronger the

**Table 2**  
Dependence of measured and estimated scintillation index reduction on coherence width in PPCBs.

Width radius [mm]	Measured reduction MR (Eq. (11)) Still [%]	Estimated reduction R (Eq. (6)) Still [%]	Measured reduction MR Eq. (11) Agitated [%]	Estimated reduction R Eq. (6) Agitated [%]
0.096	49	49	43	50
0.136	49	49	39	50
0.192	50	49	44	49
0.271	50	50	43	49
0.384	48	50	41	50
0.543	50	50	39	48
0.768	47	50	37	49
0.768 <sup>a</sup>	50	50	39	49
1.085 <sup>a</sup>	45	50	35	50

Note: Agitated conditions are with mechanically agitated fast moving scatterers.

<sup>a</sup> Change in number of cycling screens on SLM from 8000 to 2000 phase screens.

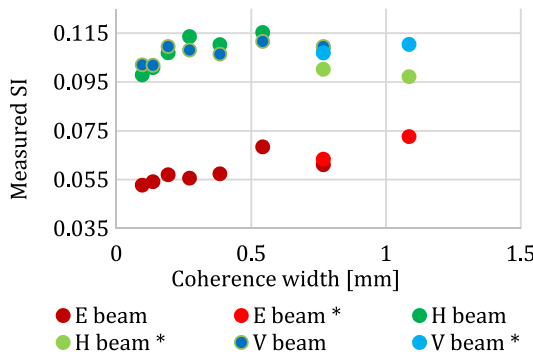


**Fig. 7.** Measured average scintillation index,  $MSI_{Bavg}$  in agitated conditions (with slow moving scatterers). Note the lower values for the electromagnetic beams and matched higher values for the scalar beams polarized vertically and horizontally. The \* denotes the change in number of cycling screens on SLM from 8000 to 2000 phase screens.

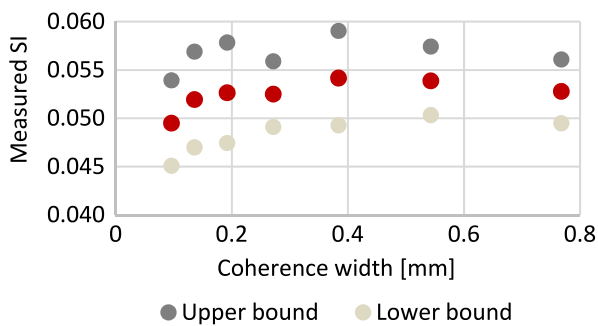


**Fig. 8.** Measured  $MSI_{Bavg}$  across the sensor area for electromagnetic beam propagating in still conditions with one standard deviation upper and lower confidence interval bounds.

scintillation is in a more complex media; but its trend also demonstrates an increase in scintillation for more spatially coherent beams relative to less spatially coherent beams. This ratio is around 1 for less spatially coherent beams, increasing to 1.5 as the beam becomes more spatially coherent. Note that the scalar beams are increasingly more prone to scintillation as they become more coherent. The deterioration of electromagnetic PPCB beams is less volatile.

If the scintillations in slow and fast moving entrained scatterer conditions are compared, the clear increase in scintillation in a more complex media is apparent. It should be noted that the construction of PPCBs through the use of the cycling of statistically prescribed phase

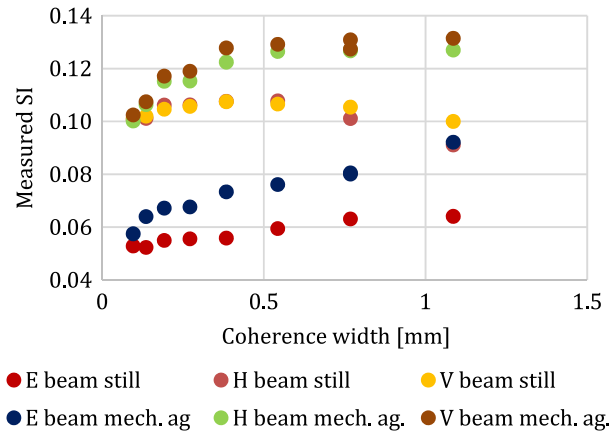


**Fig. 9.** Measured  $MSI_{Bavg}$ , comparison between the still condition and the fast moving scatterers condition as a function of coherence width values, for scalar (horizontally and vertically polarized) and electromagnetic beams.

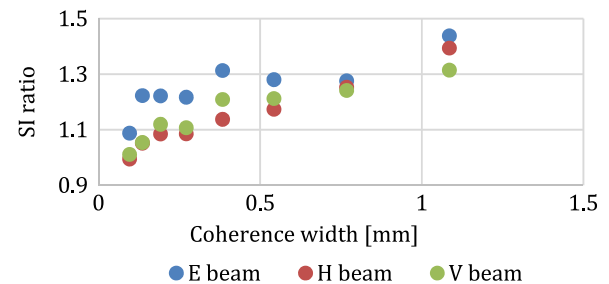


**Fig. 10.** The ratio between the fast moving scatterers condition and the still condition of  $MSI_{Bavg}$ , as a function of coherence width,  $\delta$ , for scalar (horizontally and vertically polarized) and electromagnetic beams.

screens with the SLM introduces additional fluctuations in the laser light on the target. As noted, theoretically, the cycling rate is infinite, but practically we have hardware limitations in cameras capture rate and SLM cycling rate and these instrumentation restrictions are the primary influence on the scintillation values in the still conditions. It can be observed that scintillations in the still conditions and the mechanically agitated condition where the scatterers are moving slowly are comparable in values. The reason for this effect for slow mode, is that light intensity variations due to the SLM cycling rate are dominant in comparison to the constructive and destructive interference due to the light interacting with the moving scatterers.

### 5.2. Gaussian beam

To evaluate the performance of a coherent, Gaussian laser beam, six sets of experiments were recorded: three under the still conditions and three in mechanically agitated (fast moving entrained scatterers) conditions.

Fig. 11a shows the comparisons of measured intensity and  $MSI_{Bavg}$  for a Gaussian beam. In Fig. 11a the measured intensity in still conditions is higher than in mechanically agitated conditions, and this is independent from the scenarios or beam intensity pattern. Electromagnetic beams carry approximately twice as much intensity since they represent the combination of the vertically and horizontally polarized scalar beams. In still conditions the electromagnetic beams have a slightly higher intensity, 3.5%, than their scalar combination. In the mechanically agitated conditions the intensities match within 0.7%.

In Fig. 11b, the measured  $MSI_{Bavg}$  clearly shows an increase in scintillation for mechanically agitated conditions as compared to still water conditions. In mechanically agitated conditions, the improvement

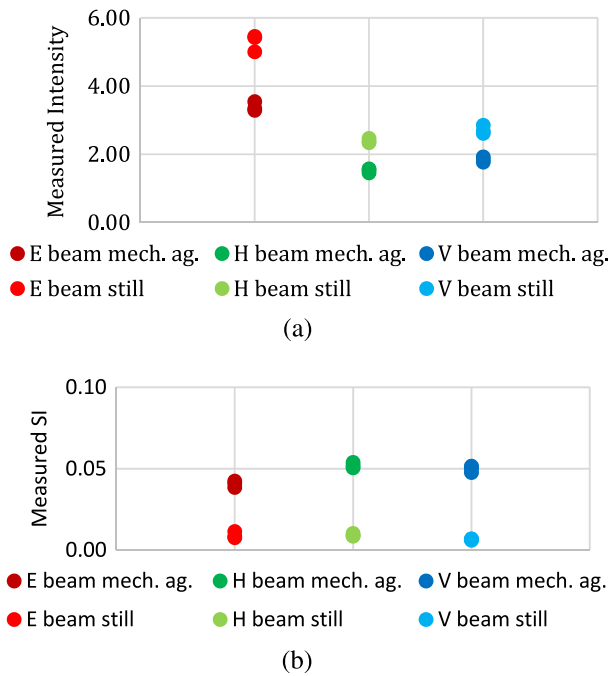


Fig. 11. Gaussian beam measurements in still and turbid conditions with mechanically agitated fast moving scatterers: (a) Measured intensity  $MI_{avg}$  and (b) Measured scintillation  $MSI_{Bavg}$ .

when an electromagnetic beam is used as compared to the scalar beam gives on average 17% in scintillation reduction. If we observe each run, the reduction is 17%, 12%, and 22% respectively, and these variations in the measurements are primarily due to the random motion of the scatterers with variable diameters moving in the water. It is significant to point out that the reduction in scintillation is not on the order of 50% as measured for PPCB. When a Gaussian beam is propagated in still conditions the reduction in scintillation is not significant, suggesting that since the measured scintillation is so low, that the benefit of propagating electromagnetic versus scalar beam is not observable.

For the electromagnetic beam, when the average measured scintillation in still water, 0.013, is compared to the average scintillation in mechanically agitated water, 0.043, the performance is 3.3 times worse in the more complex medium. In the case of scalar beams, the performance deterioration in the mechanically agitated condition is even more significant: measured  $MSI_{Bavg}$  on average going from 0.0099 in still conditions to 0.051 in mechanically agitated water, with the SI ratio being 5.1.

When the same performance metrics are compared for the fully coherent, Gaussian, electromagnetic beam (scintillation ratio from still to mechanically agitated conditions of 3.3) and electromagnetic spatially partially coherent beams (1.5) the trend strongly benefits the PPCBs.

## 6. Conclusions

We investigated the propagation of polarized spatially partially coherent and fully coherent Gaussian, laser beams underwater under two conditions: still water and mechanically agitated water with entrained scatterers.

In the case of the spatially partially coherent beams, the reduction in scintillation from propagating a scalar beam to propagating an electromagnetic beam was measured to be approximately 50% reduction in scintillation in less complex media (still water), but the performance was at the level of 40% reduction in scintillation in more complex environments (water with mechanically moving scatterers). We measured a 17% reduction in scintillation when fully coherent scalar,

Gaussian, and electromagnetic coherent beams are compared in more complex underwater media. In still conditions measured scintillations for the coherent beams was very low, and therefore the measurement uncertainty prevented a good estimate of the scintillation reduction for this case.

Furthermore, it was observed that the less coherent spatially partially coherent beams have better scintillation reduction performance as compared with more coherent beams, propagating underwater. In general, depending on the coherence width value of a partially coherent beams, the beam spreading is wider as compared to the Gaussian beam, but if the loss of the power could be normalized, the scintillation performance of the partially coherent beams appears superior.

We also established that the Gaussian beam scintillation deteriorates more rapidly as the medium becomes more complex, as compared to the spatially partially coherent beams under the same conditions underwater. It is important to note that spatially partially coherent beams have an initial intensity fluctuation due to the construction of the beam using a cycling spatial light modulator. Those induced variations are uniform across the beam cross section and become relatively negligible when laser light is propagated through a highly turbulent medium.

## Acknowledgements

S. Avramov-Zamurovic is supported by US ONR grant: N0001414-WX-00267.

C. Nelson is supported by US ONR grant N0001416WX00796.

## References

- [1] L.C. Andrews, R.L. Phillips, *Laser Beam Propagation Through Random Media*, second ed., SPIE Press, Bellingham, WA, 2005.
- [2] A. Ishimaru, *Wave Propagation and Scattering in Random Media*, Vols. 1 and 2, Academic, San Diego, Calif., 1978.
- [3] F. Wang, X. Liu, Y. Cai, Propagation of partially coherent beam in turbulent atmosphere: a review (invited review), *Prog. Electromagn. Res.* 150 (2015) 123–143.
- [4] V.A. Banakh, V.M. Buldakov, Effect of the initial degree of spatial coherence of a light beam on intensity fluctuations in a turbulent atmosphere, *Opt. Spectrosc.* 55 (1983) 707–712.
- [5] J.C. Ricklin, F.M. Davidson, Atmospheric turbulence effects on a partially coherent gaussian beam: implications for free-space laser communication, *J. Opt. Soc. Amer.* A 19 (2002) 1794–1802.
- [6] J.H. Churnside, Aperture averaging of optical scintillations in the turbulent atmosphere, *Appl. Opt.* 30 (1991) 1982–1994.
- [7] S. Rosenberg, M.C. Teich, Photocounting array receivers for optical communication through the lognormal atmospheric channel 2: optimum and suboptimum receiver performance for binary signaling, *Appl. Opt.* 12 (1973) 2625–2634.
- [8] E.J. Lee, V.W.S. Chan, Part 1: optical communication over the clear turbulent atmospheric channel using diversity, *IEEE J. Sel. Areas Commun.* 22 (2004) 1896–1906.
- [9] G.P. Berman, A.R. Bishop, B.M. Chernobrod, D.C. Nguyen, V.N. Gorshkov, Suppression of intensity fluctuations in free space high-speed optical communication based on spectral encoding of a partially coherent beam, *Opt. Commun.* 280 (2007) 264–270.
- [10] G.P. Berman, A.A. Chumak, Influence of phase-diffuser dynamics on scintillations of laser radiation in Earth's atmosphere: long-distance propagation, *Phys. Rev. A* 79 (2009) 063848–063854.
- [11] O. Korotkova, Scintillation index of a stochastic electromagnetic beam propagating in random media, *Opt. Commun.* 281 (2008) 2342–2348.
- [12] Y. Gu, O. Korotkova, G. Gbur, Scintillation of nonuniformly polarized beams in atmospheric turbulence, *Opt. Lett.* 34 (2009) 2261–2263.
- [13] X. Xiao, D. Voelz, Wave optics simulation of partially coherent and partially polarized beam propagation in turbulence, in: *Proc. SPIE 7464, Free-Space Laser Communications IX*, 74640T, Aug 21, San Diego, CA, 2009.
- [14] F. Schill, U.R. Zimmer, J. Trumpf, Visible spectrum optical communication and distance sensing for underwater applications, in: *Proc. Australasian Conf. Robot. Autom.*, 2004.
- [15] N. Farr, J. Ware, C. Pontbriand, T. Hammar, M. Tivey, Optical communication system expands CORK seafloor observatory's bandwidth, in: *Proc. OCEANS Conf.*, 2010.
- [16] M. Doniec, C. Detweiler, I. Vasilescu, D. Rus, Using optical communication for remote underwater robot operation, in: *IEEE/RSJ International Conference on Intelligent Robots and Systems*, 2010.

- [17] B. Cochenour, A. Laux, L. Mullen, Temporal dispersion in underwater laser communication links: Closing the loop between model and experiment, in : Proceedings Underwater Communications and Networking Conference (UComms), IEEE Third, 2016.
- [18] O. Korotkova, N. Farwell, E. Shchepakina, Light scintillation in oceanic turbulence, *Waves Random Complex Media* 22 (2) (2012) 260–266.
- [19] Y. Wu, Y. Zhang, Y. Zhu, Average intensity and directionality of partially coherent model beams propagating in turbulent ocean, *J. Opt. Soc. Am. A* 33 (8) (2016) 1451–1458.
- [20] S. Avramov-Zamurovic, C. Nelson, S. Guth, O. Korotkova, R. Malek-Madani, Experimental study of electromagnetic Bessel-Gaussian Schell Model beams propagating in a turbulent channel, *Opt. Commun.* 359 (2016) 207–215.
- [21] S. Avramov-Zamurovic, C. Nelson, R. Malek-Madani, O. Korotkova, Polarization-induced reduction in scintillation of optical beams propagating in simulated turbulent atmospheric channels, *Waves Random Complex Media* 24 (4) (2014) 452–462.
- [22] S. Avramov-Zamurovic, O. Korotkova, C. Nelson, R. Malek-Madani, The dependence of the intensity PDF of a random beam propagating in the maritime atmosphere on source coherence, *Waves Random Complex Media* 24 (2014) 69–82.
- [23] O. Korotkova, S. Sahin, E. Shchepakina, Multi-Gaussian schell-model beams, *J. Opt. Soc. Am. A* 29 (2012) 2159–2164.
- [24] D. Voelz, K. Fitzhenry, Pseudo-partially coherent beam for free-space laser communication, *Proc. SPIE* 5550 (2004) 218–224.
- [25] Z. Mei, O. Korotkova, E. Shchepakina, Electromagnetic multi-gaussian schell-model beams, *J. Opt.* 15 (2013) 025705.
- [26] T. Shirai, O. Korotkova, E. Wolf, A method of generating electromagnetic Gaussian Schell model beams, *J. Opt. A: Pure Appl. Opt.* 7 (2005) 232–237.
- [27] A.S. Ostrovsky, G. Rodríguez-Zurita, C. Meneses-Fabián, M.Á. Olvera-Santamaría, C. Rickenstorff-Parrao, Experimental generating the partially coherent and partially polarized electromagnetic source, *Opt. Express* 18 (2010) 12864–12871.
- [28] E. Wolf, Unified theory of coherence and polarization of random electromagnetic beams, *Phys. Lett. A* 312 (2003) 263–267.
- [29] G. Gbur, T.D. Visser, The structure of partially coherent fields, *Prog. Opt.* 55 (2010) 285.
- [30] F. Gori, Matrix treatment for partially polarized, partially coherent beams, *Opt. Lett.* 23 (1998) 241–243.
- [31] S. Sahin, O. Korotkova, Light sources generating far fields with tunable flat profiles, *Opt. Lett.* 37 (2012) 2970–2972.
- [32] M.W. Hyde IV, S. Basu, X. Xiao, D. Voelz, Producing any desired far-field mean irradiance pattern using a partially-coherent schell-model source, *J. Opt.* 17 (2015) 055607.
- [33] M.W. Hyde, S. Basu, X. Xiao, D.G. Voelz, Producing any desired far-field mean irradiance pattern using a partially-coherent Schell-model source and phase-only control, *Imaging and Applied Optics 2015 OSA Technical Digest (online)* (Optical Society of America), paper PW3E.2. (2015).
- [34] M.W. Hyde, S. Basu, D.G. Voelz, X. Xiao, Experimentally generating any desired partially coherent schell-model source using phase-only control, *J. Appl. Phys.* 118 (2015) 093102.
- [35] S. Avramov-Zamurovic, C. Nelson, S. Guth, O. Korotkova, Flatness parameter influence on scintillation reduction for multi-Gaussian Schell-model beams propagating in turbulent air, *App. Opt.* 55 (13) (2016) 3442–3446.
- [36] Y. Baykal, H.T. Eyyuboğlu, Y. Cai, Scintillations of partially coherent multiple Gaussian beams in turbulence, *App. Opt.* 48 (10) (2009) 1943–1954.
- [37] C. Mujaat, A. Dogariu, Statistics of partially coherent beams: a numerical analysis, *J. Opt. Soc. Amer. A* 21 (6) (2004) 1000–1003.
- [38] E. Hecht, *Optics*, fourth ed., Pearson Addison Wesley, 2002.
- [39] S. Avramov-Zamurovic, C. Nelson, Experimental study on off-axis scattering of flat top partially coherent laser beams when propagating under water in the presence of moving scatterers, *Waves in Random and Complex Media*, 2017.
- [40] S. Avramov-Zamurovic, C. Nelson, Experimental analysis of laser beams with variable spatial coherence propagating underwater. In: *Imaging and Applied Optics 2017 (3D, AIO, COSI, IS, MATH, pcAOP)*, OSA Technical Digest (online) (Optical Society of America, paper PTh1D.3, 2017.
- [41] C. Nelson, S. Avramov-Zamurovic, O. Korotkova, S. Guth, R. Malek-Madani, Scintillation reduction in pseudo Multi-Gaussian Schell Model beams in the maritime environment, *Opt. Commun.* 364 (2016) 145–149.